Numerical Investigation of Opposing Dual Sided Microscale Laser Shock Peening

Yajun Fan

Youneng Wang

Sinisa Vukelic

Y. Lawrence Yao

Department of Mechanical Engineering,
Columbia University,
New York, NY 10027

Laser shock peening (LSP) is an innovative process which imparts compressive residual stresses in the processed surface of metallic parts to significantly improve fatigue life and fatigue strength of this part. In opposing dual sided LSP, the workpiece can be simultaneously irradiated or irradiated with different time lags to create different surface residual stress patterns by virtue of the interaction between the opposing shock waves. In this work, a finite element model, in which the hydrodynamic behavior of the material and the deviatoric behavior including work hardening and strain rate effects were considered, was applied to predict residual stress distributions in the processed surface induced under various conditions of the opposing dual sided microscale laser shock peening. Thus the shock waves from each surface will interact in different ways through the thickness resulting in more complex residual stress profiles. Additionally, when treating a thin section, opposing dual sided peening is expected to avoid harmful effects such as spalling and fracture because the pressures on the opposite surfaces of the target balance one another and prohibit excessive deformation of the target. In order to better understand the wave–wave interactions under different conditions, the residual stress profiles corresponding to various workpiece thicknesses and various irradiation times were evaluated. [DOI: 10.1115/1.2540771]

Introduction

Since the first experiments in the 1960s utilizing high power pulsed lasers to generate shock waves in solid targets, the laser shock technique has led to many investigations. LSP was initially developed approximately 30 years ago and is now emerging as a reliable surface treatment method. Similar to traditional shot peening (SP), LSP is an innovative surface treatment technique, which has been successfully applied to improve fatigue performance of metallic components. The key beneficial characteristic after LSP treatment is the presence of compressive residual stresses beneath the treated surface of metallic materials, mechanically produced by high magnitude shock waves induced by a high-energy laser pulse. Compared with the traditional shot peening process LSP can produce high magnitude compressive residual stresses of more than 1 mm in depth, four times deeper than traditional SP [1]. LSP has been intensively investigated in the last 2 decades. Most studies and investigations are based on experimental approaches, focusing on understanding mechanisms of LSP and its influences on mechanical behaviors and in particular enhanced fatigue performance of treated metallic components. In most cases, there was a lack of comprehensive documentation in the relevant information in applications of LSP for various metallic alloys, such as material properties, component geometry, laser sources, and LSP parameters. However, some comprehensive modeling capacities based on analytical models and dynamic finite element models (FEM) have been established for simulating LSP in the last decade, which provide unique tools for evaluation of LSP and optimization of residual stress distributions in relation to material properties, component geometry, laser sources, and LSP parameters. Those approaches can play significant roles in design and optimization of LSP processes in practical applications.

In LSP, laser-generated shock waves result from the expansion of a high pressure plasma caused by a pulsed laser. An intense laser pulse interacting with a solid target immediately causes the surface layer to instantaneously vaporize into a high temperature and high pressure plasma. This ablated plasma expands from the surface and, in turn, exerts mechanical pressure on the face of the target, which induces compressive waves in the solid target, and therefore a shock wave is propagated through the sample. If it is confined by liquid or another type of laser transparent medium, the shock pressure can be magnified by a factor of 5 or more compared with the open-air condition [2]. The coating also protects the target from thermal effects so that nearly pure mechanical effects are induced. When the peak pressure created by the shock wave is above the dynamic yield stress of metal, the metal is plastically deformed at the surface which will induce compressive residual stress in the surface of the part and thus increase the resistance of the metal to surface related failures such as fatigue, fretting fatigue, and stress corrosion cracking. LSP has been extensively investigated and successfully applied in some cases [3–8].

Because of large pressures involved in LSP, one-sided laser shock peening on thin targets can result in significant permanent deformation or spall failure on the backsurface. Generally when treating a thin section, opposing dual sided pending is used to avoid harmful effects such as spalling and fracture. Opposing dual sided laser shock peening is accomplished by splitting the laser beam in half and peening both opposing surfaces of the target. The pressures on the opposite surfaces of the target balance one another and prohibit excessive deformation of the target. More recently, various methods of opposing dual sided irradiation [9] are provided to establish selective compressive residual stress profiles within a workpiece, i.e., simultaneous irradiation or irradiation with different times. Thus the shock waves from each surface will interact in different ways through the thickness resulting in more complex residual stress profiles. To gain control on the resulting residual stress distributions in different irradiation methods we need to better understand wave–wave interactions in opposing dual sided LSP (Fig. 1).

Numerical modeling is an effective way to understand wave–wave interaction in solids. Shock wave propagation in solids has

Contributed by the Manufacturing Engineering Division of ASME for publication in the JOURNAL OF MANUFACTURING SCIENCE AND ENGINEERING. Manuscript received February 6, 2006; final manuscript received August 30, 2006. Review conducted by Kamlakar Rajurkar.

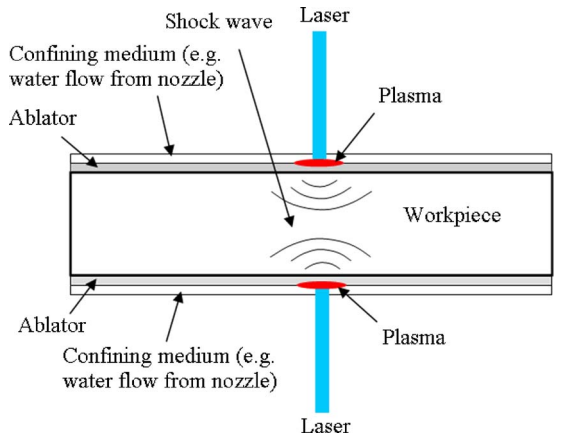

Fig. 1 Schematic of opposing dual sided laser shock peening

been numerically investigated [10–12]. Mok [10] simulated the propagation and attenuation of spherical and plane shock waves in a 2024 aluminum plate by assuming that the media is a strain-rate-independent and elastic-perfectly plastic solid. Caruso et al. [11] also numerically investigated laser-generated shock propagation dynamics in the solids, but only an elastic medium in plane geometry was considered. Shock-solid interaction was also simulated in some studies of spallation and residual stresses induced by LSP [12], but the effect of high strain rate was not considered or fully considered only by the Johnson–Cook law.

Microscale laser shock peening has been well studied by both numerical and experimental ways in Columbia University [5,6,13]. In this work, a well validated explicit/implicit FEM model [14], in which the hydrodynamic behavior of the material and the deviatoric behavior considering work hardening and strain rate effects were considered, is applied to investigate the wave–wave interactions in various microscale laser shock peening methods. In this model, explicit dynamic analysis is implemented for shock wave propagation in strain-rate dependent and elastic-plastic solids and implicit analysis is applied for relaxation of pressured materials. By simulation, opposite sides of the workpiece with different thicknesses are irradiated simultaneously or at different times and the final residual stress distributions within the workpiece are calculated. In this study, the effects of irradiation methods, thickness, and pulse duration will be numerically analyzed. Based on the analysis of the wave–wave interaction, the optimal processing methods to selectively modify in a controlled manner the compressive stress distribution profile are developed.

Mathematical Model

Shock wave plays an important role in LSP. When a high pressure is suddenly applied to a metallic target, the pressure is accumulated in the wave front because it cannot disperse away within such a short time, and thus an almost discontinuous jump of pressure, density, and internal energy is formed across the wave front. A shock wave is then formed. Shock waves are characterized in that the wave front is a region of sudden and violent change in pressure, material internal energy, and density. The shocked solids are thought to have a fluidlike hydrodynamic deformation under such a high pressure, but solids are still different from liquids in that solids have material strength and plastic flow and their deformation behavior is also related to strain and strain rate in particular.

Governing Equations. The precise numerical description of a LSP process requires the simulation to take into account the hydrodynamic behavior of the material and the deviatoric behavior considering work hardening and strain rate effects. The calculations of dynamic behavior of condensed matter under shock loading was made using the three conservation equations of mass, momentum, and energy. But these conservation laws cannot completely govern the behavior of solids under shock loading. When the applied stress greatly exceeds the yield stress of a solid, its behavior is more complicated, and can be approximated by a fluidlike one because the fractional deviations from stress isotropy are small. The complete process of shock wave propagation in solids should be governed by the three conservation equations, equation of state that can be expressed in terms of specific internal energy as a function of pressure and density for hydrodynamic behavior of material, and the elastic-plastic constitutive relation for deviatoric behavior.

The calculation of mechanical behavior of solids under shock loading is usually made using the three conservation equations in integral forms

$$\frac{d}{dt}\int_V \rho dV = 0 \tag{1}$$

$$\frac{d}{dt}\int_V \rho u_i dV = \int_S \sigma_{ij} u_j dS \tag{2}$$

$$\frac{d}{dt}\int_V \rho\left(E + \frac{1}{2}u^2\right)dV = \int_S \sigma_{ij} n_{jk} u dS \tag{3}$$

where V is the volume of a cell, S is the surface that covers this volume, n_{ij} is the unit vector normal to this surface, u_i is the velocity component, E is internal energy, and σ_{ij} is the stress components. The elastoplastic behavior should also be considered except the hydrodynamic change of volume or density. The stress-tensor components are divided into a hydrostatic equation of state and an elastic-plastic constitutive model. The stress components σ_{ij} can be written as

$$\sigma_{ij} = -P + s_{ij} \tag{4}$$

where P is the hydrostatic pressure and s_{ij} is the deviatoric stress components.

A commonly used equation of state for solids is the Mie–Grüneisen equation of state. The Mie–Grüneisen equation of state which establishes a relationship between pressure P and internal energy E with reference to the material Hugoniot curve, was used

$$P - P_H = \gamma_0 \rho_0 (E - E_H) \tag{5}$$

where P_H and E_H are the Hugoniot pressure and internal energy, γ_0 is a material constant, and ρ_0 represents the initial state density.

The Hugoniot curve is described by the linear relation between the shock velocity U and particle velocity u with coefficients from experimental data [15]

$$U = C_0 + Su \tag{6}$$

where the constant C_0 is the sound speed at zero pressure and the material constant S has a value between 1.0 and 1.7 for most metals.

Combining Eq. (6) with the Rankine–Hugoniot jump conditions [16], the Hugoniot pressure and internal energy can be obtained as

$$P_H = \frac{\rho_0 C_0 \eta}{(1 - S\eta)^2} \tag{7}$$

$$E_H = \frac{P_H \eta}{2\rho_0} \tag{8}$$

and substituting Eqs. (7) and (8) into Eq. (5) yields

$$P = \frac{\rho_0 C_0 \eta}{(1 - S\eta)^2}\left(1 - \frac{\gamma_0 \eta}{2}\right) + \gamma_0 \rho_0 E \tag{9}$$

where $\eta = 1 - \rho_0/\rho$, and ρ is density. Equation (9) is the final form of equation of state to be used in this simulation. In the following numerical modeling of shock-solid interactions, work hardening,

strain rate, and pressure effects on yield strength are considered while temperature is taken as room temperature. This is reasonable because only the coating is vaporized and minimal thermal effects are felt by the sample. The solid target is assumed to be isotropic.

Laser-Generated Shock Loading. Previous shock pressure models [8] assumed that a certain amount of plasma exists instantaneously once the laser is on. A constant fraction of plasma internal energy α was assumed to increase the pressure of the plasma. The way in which α was experimentally determined is rather cumbersome and indirect, and therefore most literature reported a constant value for different laser intensities. This value also varied from 0.1 to 0.4 across different literature. The reason is that in previous models there was no consideration of mass exchanges between plasma and confining medium (e.g., water) or plasma and target, only energy and momentum conservation were considered. Explicit consideration of the mass transfer in the model will eliminate the need for prescribing the value of α and thus reduce the arbitrariness and increase the model accuracy, which is crucial for the microscale under consideration. A model [17] has been developed for the prediction of laser-generated pressure in the confined ablation mode. It considered the mass, energy, and momentum exchanges between plasma and confining medium or plasma and metallic target. The expansion of plasma was modeled as one-dimensional laser-supported combustion wave. The obtained one-dimensional results were then modified to consider spatial expansion effects of the shock pressure. The calculated shock loading was used in the later shock wave propagation simulation as input and was assumed to be of a spatially Gaussian distribution.

Materials Model. In LSP, the target is subjected to very strong shock pressures (>1 GPa), the interaction time is very short (<200 ns), and the strain rate is very high ($>100{,}000\ s^{-1}$). At such strain rates, metals behave significantly different from under quasi-static conditions. If it is assumed that the yielding occurs when the peak stress in the longitudinal wave reaches the Hugoniot elastic limit (HEL), then the dynamic yield strength (Y) under uniaxial stress conditions can be expressed in terms of HEL by

$$Y = \frac{1-2\nu}{1-\nu}\mathrm{HEL} \tag{10}$$

where ν is the Poisson's ratio. Since the HEL is not rate dependent, it has been assumed that this material behaves as elastic-perfectly plastic with a yield strength defined by Eq. (10). However, it is accurate to assume that it is under uniaxial stress conditions in LSP. For example, in LSP, surface waves are also generated around the perimeter of the laser beam spot. It is necessary to consider the effect of high strain rate on the flow behavior of metals. Johnson et al. [18] first included the influence of strain rate $\dot{\varepsilon}$ into their working hardening model. But Johnson's model [18] could not cover the high strain rate (greater than $10^{-6}\ s^{-1}$) in LSP. It did not also consider pressure effects, which are very important in laser shock processing. Steinberg's model [19] is applicable to ultrahigh pressures but it did not consider rate dependent effects. It was found that the rate dependent effects cannot be neglected for shock pressures below 10 GPa. In laser shock processing, the pressure involved is fairly high (>1 GPa) but less than 10 GPa.

For laser shock processing, therefore, both the strain rate effects and ultrahigh pressure effects on material yield stress need to be considered. A prior research [5] has included the strain rate (even above $10^{6}\ s^{-1}$) effects and ultrahigh pressure effects on material yield stress, and the obtained dynamic yield stress data were used in this research.

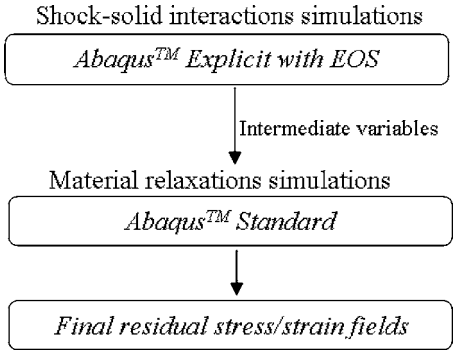

Fig. 2 The FEM simulation chart for microscale LSP

Numerical Modeling

FEM Explicit and Implicit Modeling. The commercial finite element solver, ABAQUS/Explicit and ABAQUS/Standard, were combined to perform the LSP simulation. These two solvers accomplish different calculations during this simulation. The ABAQUS/Explicit is a nonlinear explicit time integration finite element code, which requires very small time steps and is especially well suited for solving high speed, short duration, highly dynamic events that require many small time step increments to obtain a high resolution solution. The ABAQUS/Standard is a nonlinear elastic-plastic implicit time integration finite element code used primarily for static or natural frequency calculations. The two finite element solvers are applied together to provide the most effective and efficient numerical solution. One important issue about the simulation of LSP is the balance between a short time for dynamic shock-solid interaction (2–3 times of the laser pulse duration) and a much longer relaxation time (up to 1 s) to reach a stabilized mechanical state. So the ABAQUS/Explicit code is first applied to simulate the dynamic shock-solid interaction process. But the ABAQUS/Explicit method is only conditionally stable and very small time step is required. Therefore, the second step is to simulate material relaxation in ABAQUS/Standard. As soon as the calculation of the highly dynamic shock-solid interaction process is completed in ABAQUS/Explicit, the obtained intermediate stress and strain state is transferred into ABAQUS/Standard to simulate the material relaxation and get the residual stress filed in static equilibrium. The implementation chart of simulation is shown in Fig. 2 In the dynamic explicit analysis step, equation of state (Eq. (9)) will be incorporated into conservation laws and the elastic-plastic constitutive model to describe the pressure-volume-energy relation of material under shock loading. In the ABAQUS/Explicit step, a small amount of damping in a form of bulk viscosity (=0.06) is included in the calculation to limit numerical oscillations.

To accurately capture the residual stress field it is necessary to have sufficient mesh density within the finite element model. Fine elements were used to model the area around the shock load, and the elements were biased laterally and vertically away from the load center (Fig. 3) The finest grid is around 0.4 μm. The axis-symmetric boundary conditions are applied in the modeling of LSP, and element type is CAX4R.

Simulation Conditions. In the simulations, the processing conditions are just similar to prior works [14]: the laser duration time is 50 ns, beam spot size diameter is 12 μm, the laser intensity is 4.95 GW/cm^2, and the corresponding pulse energy is 280 μJ. The material is assumed to be isotropic. Only room temperature is considered because most heat generated by coating layer ablation is shielded from the target by the layer in practical operation of LSP. Table 1 gives the mechanical properties of studied copper in this work.

As mentioned above, the surface residual stress distributions

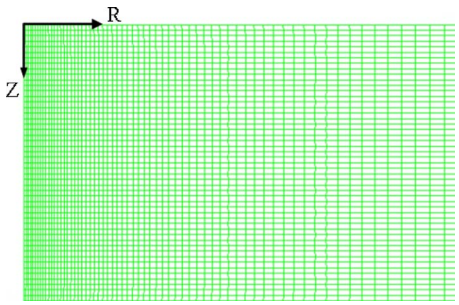

Fig. 3 Mesh of finite element model for dual sided laser shock peening with axis-symmetric condition

are closely relative to the wave–wave interactions in opposing dual sided irradiation LSP. To investigate the effect of thickness on the wave–wave interactions, two different thicknesses are considered in the simulations: 100 and 200 μm. In the simulations, various radiation methods are investigated. Figure 4 shows the studied irradiation methods in this work. In Fig. 4, zero phase represents simultaneous irradiation; half phase refers to the case in which as one shock wave moves to the mid-plane of the plate, the other laser beam irradiates; and in full phase as one shock wave travels through the whole thickness of the plate, the other laser beam irradiates.

Results and Discussions

Dual Sided Irradiation and One Sided Irradiation. To understand how the wave–wave interactions in dual sided irradiation LSP influences the resulting residual stresses distribution, the simulated surface residual stress profiles in zero phase LSP and one sided irradiation LSP are compared. The numerical conditions have been given in the section of numerical modeling. Figure 5 shows that the comparison of the calculated top surface residual stresses between one sided irradiation and zero phase dual sided irradiation. It should be noted that the residual stress is an average residual stress in the depth penetration of 20 μm because the penetration depth of X-ray in aluminum around 20 μm when X-ray diffraction is applied to measure residual stress distribution. In Fig. 5, the calculated surface residual stress (σ_R) is not decreasing from the irradiated center to the perimeter of the shocked area. In the center, the surface residual stress is the most compressive, and

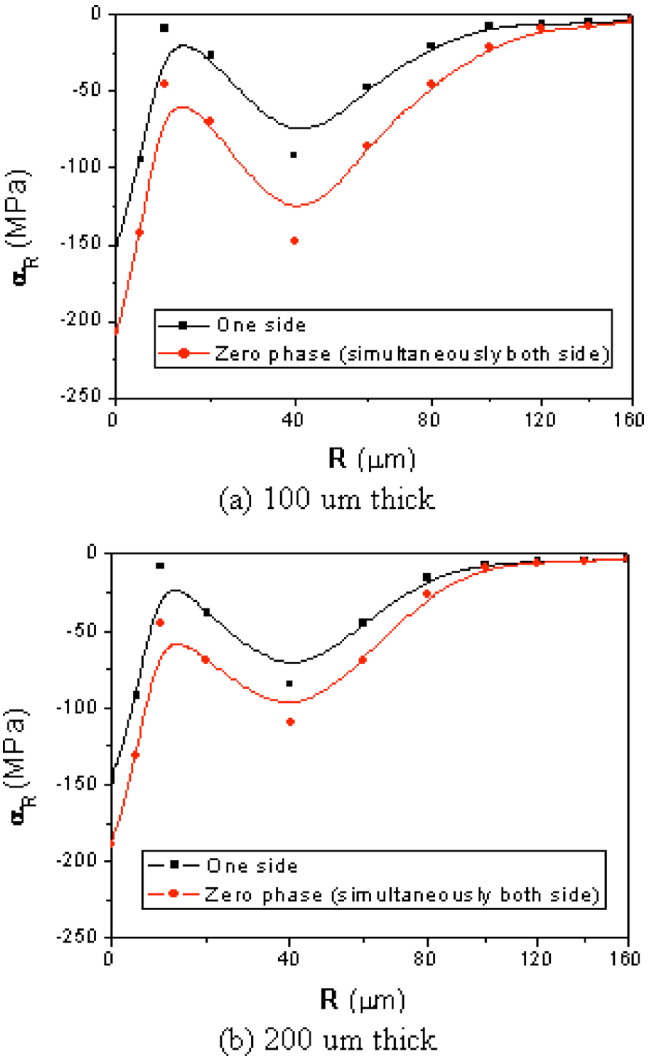

Fig. 5 Comparison of the calculated top surface residual stresses between one sided irradiation and zero phase dual sided irradiation in the samples with different thickness: (*a*) 100 and (*b*) 200 μm thick. Laser intensity is 4.95 GW/cm^2, beam spot size is 12 μm, and pulse duration is 50 ns.

Table 1 Mechanical properties of studied material

Parameters	Copper
Density ρ_0 (kg/m^3)	9860
Shear modulus G (MPa)	468
Sound speed at zero pressure C_0 (m/s)	3940
Particle velocity coefficient S	1.489
Grüneisen coefficient γ_0	1.99
Poisson's ratio ν	0.38

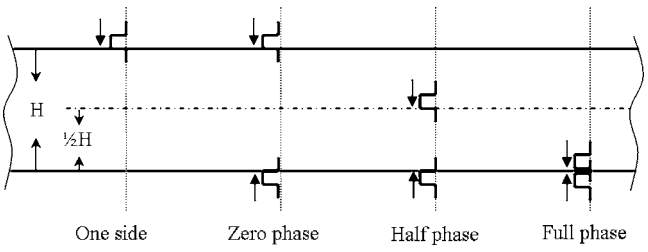

Fig. 4 Schematic of various irradiation methods in LSP. *H* is the thickness of the processed thin section.

becomes much less compressive or slightly tensile in the area about 20 μm far from the center, and then in the farther area from the center the surface residual stress comes to be very compressive again. This kind of surface residual stress profile is also found in other works [1,4–6]. The reason why near the edge of laser irradiation is less compressive or slightly tensile is that under shock loading the shocked surface is elongated and the elongation mainly takes place around the laser irradiated spot, and therefore this area becomes much less compressive and sometimes tensile.

From Fig. 5, it is found that in zero phase dual sided irradiation the top surface residual stresses are enhanced for both 200 and 100 μm thick samples. An increase by up to 33% of residual stresses in magnitude is obtained. This enhancement of the surface compressive residual stress in the zero phase dual sided irradiation is clearly due to the shock–shock interactions. In addition, the surface residual stress distribution is wider in the zero phase dual sided irradiation than that in one sided irradiation because the wave–wave interaction in zero phase dual sided irradiation is weaker in a thicker plate (200 μm). In zero phase dual sided irradiation LSP, the shock wave from the top surface will meet the shock incident from the bottom surface at the midplane and the encountering shock waves will interact in a manner generally ex-

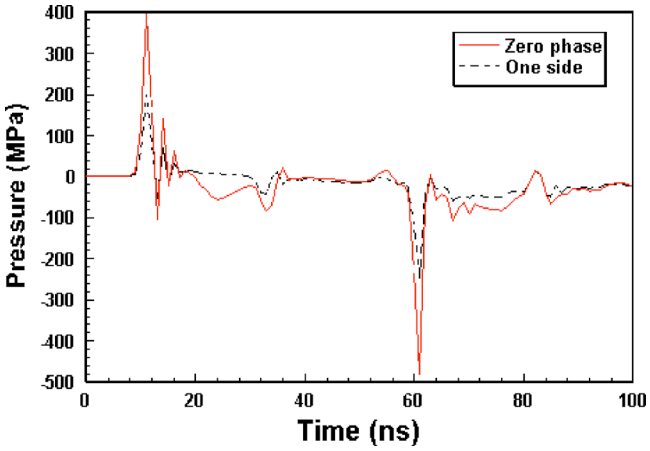

Fig. 6 Comparison of the time history of pressure at the central point in the midplane between one sided irradiation and the zero phase dual sided irradiation on the 100 μm thick plate. Laser intensity is 4.95 GW/cm^2, beam spot size is 12 μm, and pulse duration is 50 ns.

hibiting a constructive interference effect. In this manner, the respective deep compressive residual stress regions that extend from each of the adjacent nonoverlapping laser shock peened surfaces will overlap and significantly increase the peak pressure experienced by the material in the vicinity of the shock wave intersection plane. Figure 6 gives the comparison of the time history of pressure at the central point in the midplane between the one sided irradiation and the zero phase dual sided irradiation on the 100 μm thick plate. In Fig. 6, the speed of sound in copper is about 4 μm/ns, so the first peak at about 12.5 ns shows that the shock waves pass the midplane the first time, and then are reflected and become tensile, and come back to the midplane at about 37.5 ns, which is within loading time (50 ns). The reflected tensile shock waves were offset by the on-going shock waves, so there are no enhanced peaks at 37.5 ns. After another reflection, shocks meet at the midplane again at 62.5 ns. Due to the enhancement from wave–wave interactions, the magnitude of pressure at the midplane at 12.5 and 62.5 ns in the zero phase dual sided irradiation is about twice that of the one sided irradiation.

Effect of Phase on Residual Stress Distributions. Figure 7 shows the calculated radial residual stress distributions within the 100 μm thick copper plate by various irradiation methods. From Fig. 7, dual sided irradiations gain a more compressive and wider distributed surface residual stress compared with one sided irradiation. In one sided irradiation, there is almost no surface residual stress on the bottom. In dual sided irradiations with different phases, the compressive surface residual stress profiles are also different: full phase results in the most compressive and widest surface residual stress profiles, and zero phase obtained the relatively least compressive and narrowest surface residual stress distributions. But with different phases, the penetration of surface compressive residual stresses does not show evident difference. Figure 8 also shows the calculated surface residual stress distributions at top surfaces of the 100 and 200 μm thick samples by various irradiation methods. Similar residual stress distributions were obtained at the bottom surfaces. The plotted profiles of the surface residual stresses in the 200 μm thick sample exhibits the same trend as those in the 100 μm thick sample, as shown in Fig. 7. With the change from zero phase to full phase, the compressive surface residual stresses on both the top and bottom surface becomes larger and more widely distributed, which means that different phases cause different effects of interactions between the opposing time-staggered shock waves induced by laser shock peening. But in the 100 μm thick sample, the enhancement of compressive surface residual stresses caused by wave–wave interaction is more evident under the same conditions because of more attenuation of the shock waves in a thick plate. Figure 9 shows the calculated time history of pressure at the central point in the midplane by various opposing dual sided irradiation methods on the 200 μm thick plate. It is already known that the pressure is almost doubled in the central point in the zero phase dual sided irradiation compared with one sided irradiation. From Fig. 9, for the zero phase irradiation, the first peak at about 25 ns shows that the laser

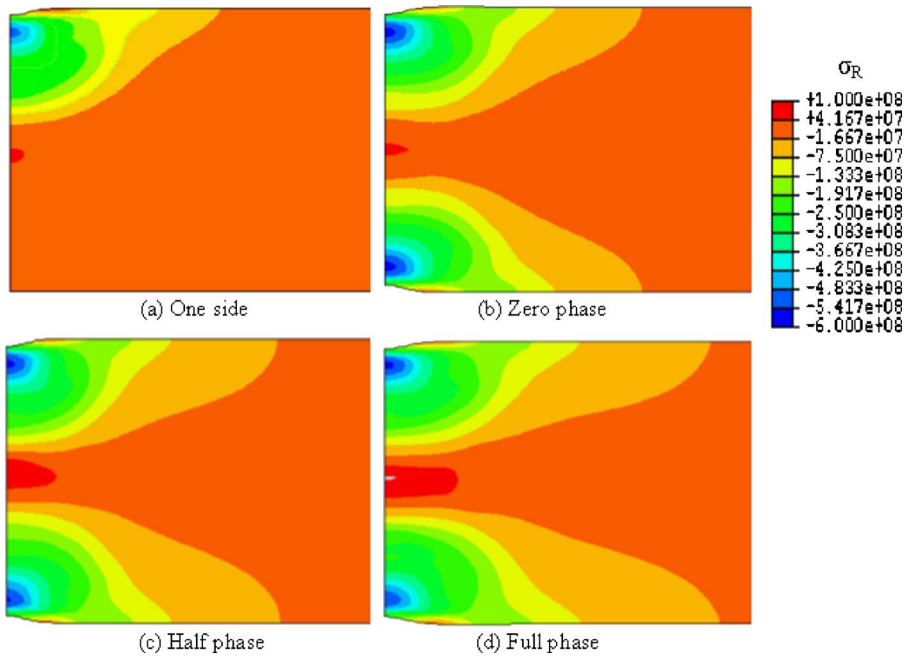

Fig. 7 The computed residual stress distributions within the 100 μm thick plate by various irradiation methods. Laser intensity is 4.95 GW/cm^2, beam spot size is 12 μm, and pulse duration is 50 ns.

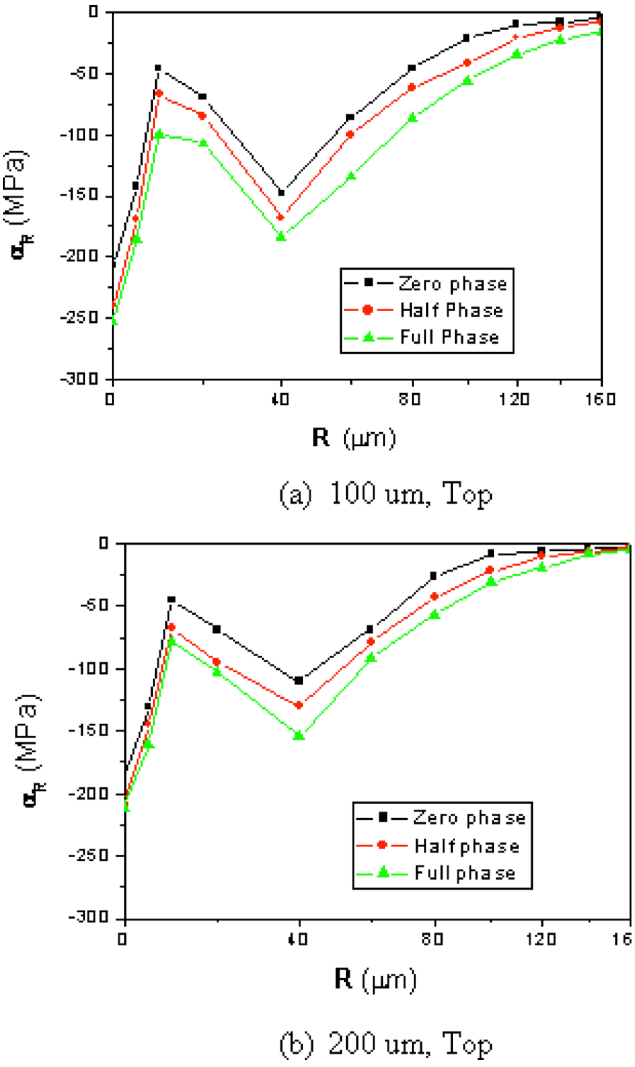

Fig. 8 The calculated top surface residual stress distributions by various phases in dual sided irradiation. Similar residual stress distributions are also found at the bottoms. Laser intensity is 4.95 GW/cm^2, beam spot size is 12 μm, and pulse duration is 50 ns.

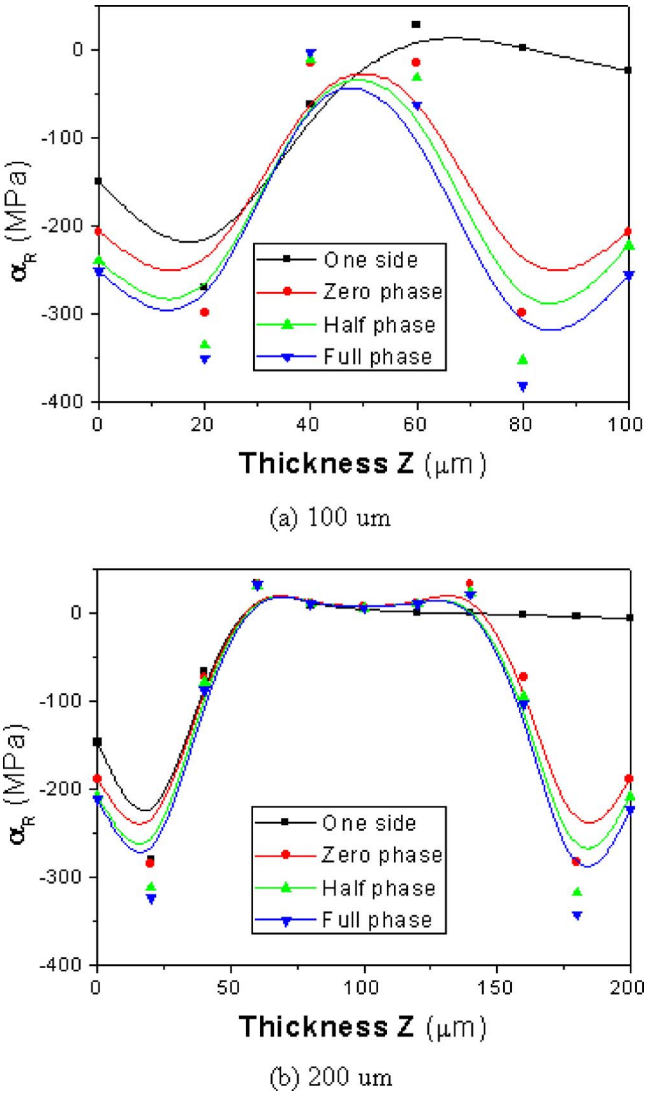

Fig. 10 The calculated residual stress distributions through the thickness at the central line of the 100 and 200 μm thick plates by various irradiation methods. Laser intensity is 4.95 GW/cm^2, beam spot size is 12 μm, and pulse duration is 50 ns.

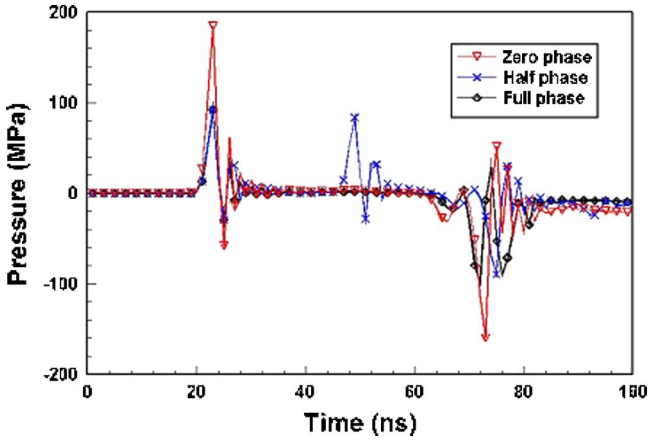

Fig. 9 Comparison of the time history of pressure at the central point in the midplane by various irradiation methods on the 200 μm thick plate. Laser intensity is 4.95 GW/cm^2, beam spot size is 12 μm, and pulse duration is 50 ns.

driven shock waves pass the midpoint the first time, and is reflected back to the midpoint at about 75 ns. For the half phase irradiation, the laser driven shock wave from the top surface goes through the midpoint at about 25 ns and the laser driven shock wave from the bottom surface reaches the midpoint at about 50 ns. In the case of half phase irradiation, although the pressure wave is not enhanced by wave–wave interaction like in the zero phase irradiation, the copper plate is just like being double irradiated by two coordinated laser pulses with the time gap of 25 ns, so the resulting surface residual stresses are also enhanced. For the full phase irradiation, the oppositely directed shock waves meet on the bottom and the interactions of waves makes the bottom surface simultaneously compressed by the two oppositely directed shock waves, so when the shock waves come back to the midpoint at about 75 ns, the interactions make the duration of pressure waves almost double wider than in the zero phase and half phase irradiations. In the full phase irradiation, the enhanced effect is the strongest because the waves meet just on the surfaces.

Figure 10 shows the calculated residual stress distributions through the thickness at the central line of the 100 and 200 μm thick copper plates by various irradiation methods. Clauer et al.

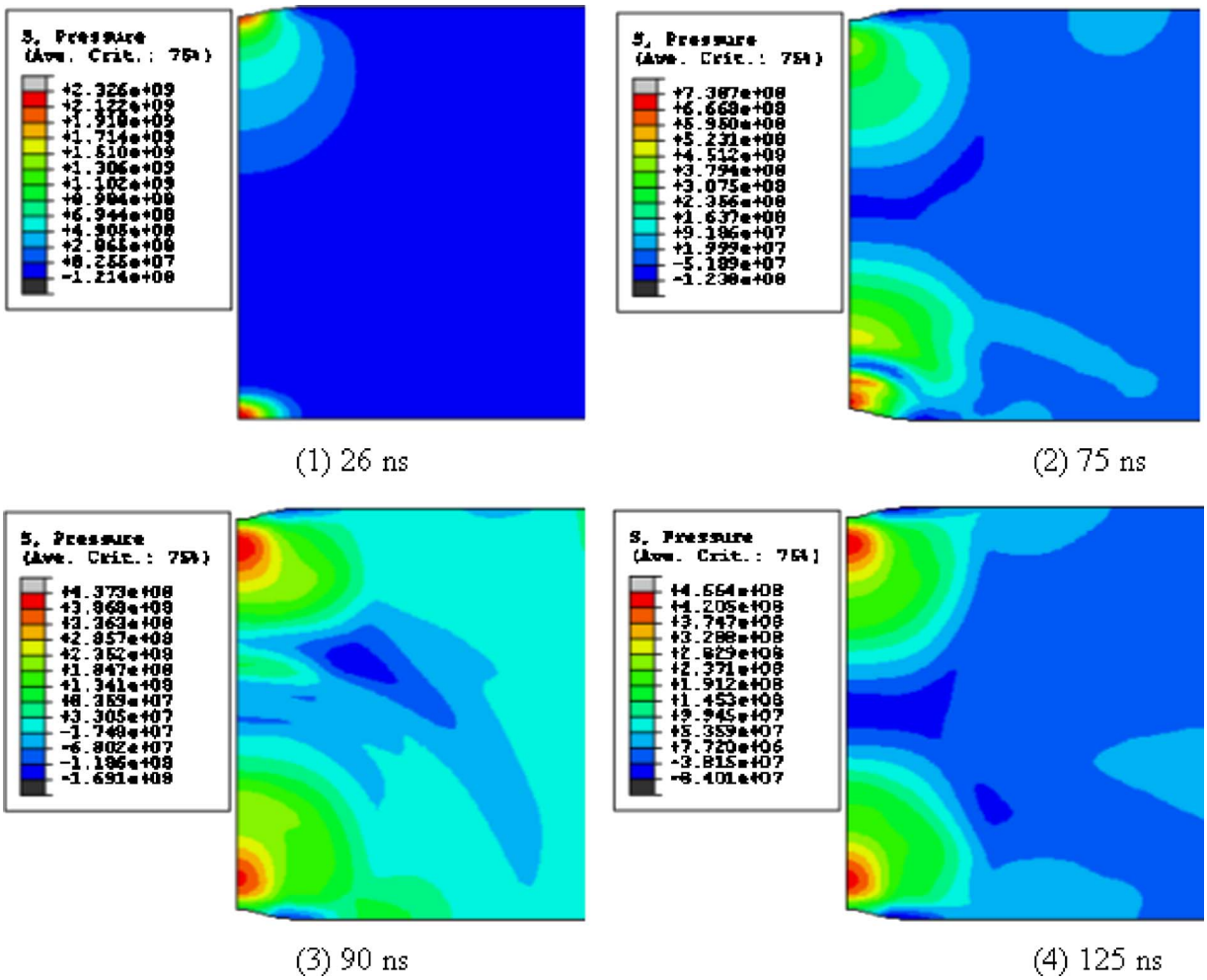

Fig. 11 Wave–wave interactions within the copper plate of 100 μm thickness by full phase irradiation. Laser intensity is 4.95 GW/cm^2, beam spot size is 12 μm, and pulse duration is 50 ns.

[9] predicted that in different phase LSP, the opposing time-staggered shock waves induced by laser shock peening would meet at a location apart from a midplane of the plate, producing an asymmetrical compressive residual stress profile through a thickness dimension of the plate. The relative difference between the arrival times of the laser beams used to laser shock peen the opposing sides of the plate could be chosen to facilitate control of the profile characteristics by selectively determining the interior location where the opposing shock waves would encounter one another. The oppositely directed shock waves would interact in a generally asymmetrical manner relative to a midplane of the plate, producing a shock wave interaction zone generally centered about the midplane but exhibiting wing-type portions that extend toward opposite ones of the plate surfaces in an oblique manner relative to the midplane. A corresponding asymmetrical stress distribution profile would accompany this particular form of shock wave interaction associated with the simultaneous formation of laterally offset laser shock peened surfaces irradiated at opposing sides of the plate. However, from Fig. 10, no evident asymmetrical stress distribution profiles are found for both thicknesses although it was found that a small shift of stress distribution towards to the bottom surface relative to the midplane. The reason why the asymmetrical stress distribution is not impressive with different phase irradiation methods in microscale LSP is that a smaller radius compact produces a stress wave which will quickly develop to propagate radically due to the quickly developed lateral waves and the interaction between lateral release waves and longitudinal shock wave makes the longitudinal shock wave attenuate more severely. The final stress distribution profile through the thickness is more dependent on the longitudinal pressures wave. So the asymmetrical stress distribution profiles through thickness in Fig. 10 are not very impressive due to quick attenuation of longitudinal shock waves. Figure 11 gives a few snapshots of wave–wave interactions within the copper plate of 100 μm thickness in full phase irradiation, showing the process of attenuation of longitudinal pressures waves and that the asymmetry of pressure distribution is gradually losing.

In addition, various forms of selective contouring and geometrical shaping can be achieved using those shock wave interaction effects in LSP by various dual phase irradiations. For example, various spatial features such as bending, deformation, and controlled curvatures can be established and formed.

Effect of Pulse Duration. In the above analysis, the duration of laser pulse is 50 ns, which is larger than the time required for shock to propagate from the top to the bottom (25 ns for 100 μm thick copper plates). To investigate the effect of pulse duration on the wave–wave interactions in various phase dual sided irradiation LSP, another case, in which the laser pulse duration is 10 ns and the sample is a 100 μm thick copper plate, is studied. In the case of 10 ns pulse duration, the same peak pressure (3 GPa) of loading is maintained and the other conditions are the same except pulse duration. The simulated residual stress distributions by zero phase and full phase irradiation methods are shown in Fig. 12. From Fig. 12, compared with the zero phase irradiation the surface compressive residual stresses in the full phase irradiation are

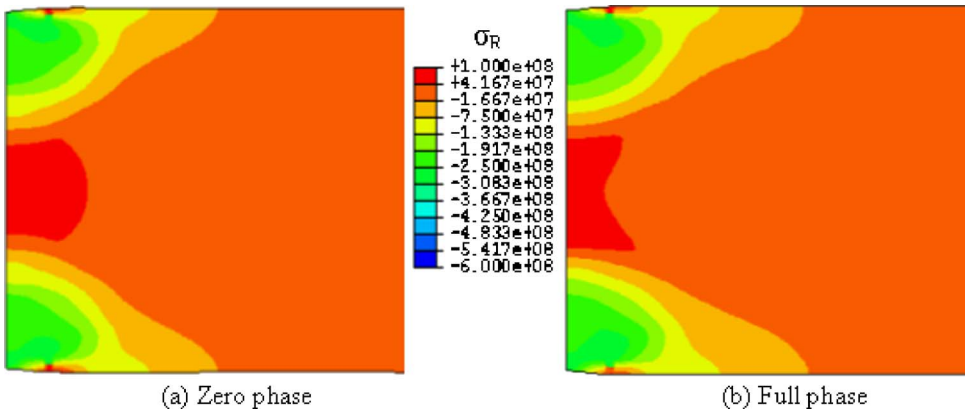

Fig. 12 The computed residual stress distributions within the 100 μm thick plate by various irradiation methods. Beam spot size is 12 μm, pulse duration is 10 ns, and the same peak pressure (3 GPa) of loading is maintained.

enhanced just like in the case of 50 ns pulse duration. However, compared with the case of 50 ns pulse duration, the obtained enhancement of compressive residual stress in the case of 10 ns pulse duration is much weaker. In Fig. 12 of the case of 10 ns pulse duration, the outer compressive stress contour in full phase irradiation becomes about 10% wider than that in zero phase irradiation, while in Fig. 7 of the case of 50 ns pulse duration, the outer compressive stress contour in full phase irradiation becomes about 40% wider than that in zero phase irradiation. Figure 13 compares the calculated pressure distributions at different time through the thickness at the central line of the 100 μm thick copper plate in full phase irradiation of microscale LSP with durations of 10 and 50 ns. In Fig. 13(*a*), the shock wave from the top surface reached the bottom at 25 ns and began to interact with the shock from the bottom surface. It has been known that an unsupported shock wave attenuates much faster than a supporting shock when other conditions are the same [14]. For the case of 10 ns pulse duration, the pressure wave was already attenuated to be very weak at 25 ns due to short supporting time (pulse duration), so strong interactions are not found in Fig. 13(*a*). It is just like that two shock waves separately propagated from the top and bottom surfaces, respectively. In Fig. 13(*b*), the shock wave from the top surface was still supported when it reached the bottom at 25 ns, therefore at 30 ns, the pressure of shock wave from the top surface was larger than that at 25 ns, which means that the shock wave from the top surface was enhanced due to the interaction with the shock from the bottom. So Fig. 13 explains why the obtained enhancement of compressive residual stress in the case of 10 ns pulse duration is much weaker than that in the case of 50 ns pulse duration.

Conclusions

In the present work, the finite element model, in which the hydrodynamic behavior of the material and the deviatoric behavior were considered, was used to investigate the resulting residual stress distributions of the processed surface under various irradiation conditions of the opposing dual sided microscale laser shock peening. In this study, the compressive surface residual stress were enhanced in the opposing dual sided irradiation comparing to that in one sided irradiation. Moreover, among opposing dual sided irradiation, the full phase irradiation obtained the strongest enhancement of surface compressive residual stress because strong shock wave–wave interactions took place right on the surface. But in full phase irradiation the asymmetric residual stress distributions through the thickness as predicted in large scale LSP was not impressive in microscale LSP because a smaller radius compact produced those quickly developed lateral waves and the attenuation of longitudinal waves came from the interactions between lateral release waves and longitudinal shock wave, which caused a weak asymmetric effect although the irradiations were opposing time triggered. It was also found that a larger thickness

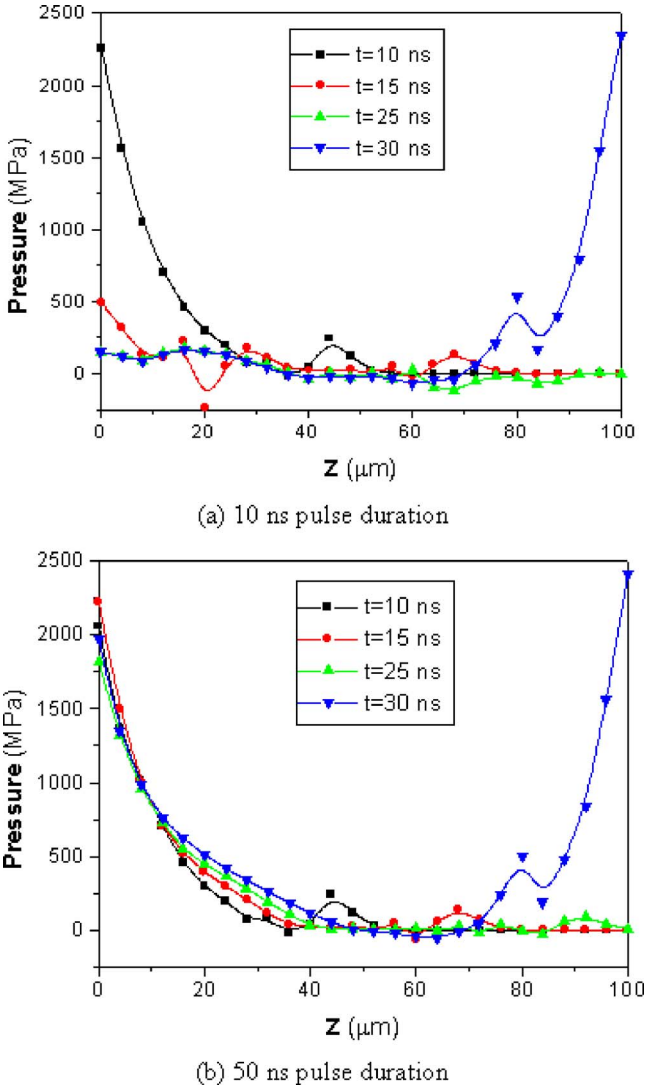

Fig. 13 Calculated pressure distributions through the thickness at the central line of the 100 μm thick plate in full phase irradiation of micro scale LSP with durations of 10 and 50 ns

of the samples caused a severe attenuation of shock waves before interactions and a weaker interaction of waves, producing a less enhancement of surface compressive residual stresses. Similarly, for shorter laser pulse duration, the quicker attenuation of shock waves also made the wave–wave interactions weaker, leading to a less strong surface compressive residual stresses. The analysis in this work can be applied for selectively inducing various surface residual stress profiles in LSP corresponding to needs.

References

[1] Clauer, A. H., and Lahrman, D. F., 2001, "Laser Shock Processing as a Surface Enhancement Process," Key Eng. Mater., **197**, pp. 121–144.

[2] Fox, J. A., 1974, "Effect of Water and Paint Coatings on Laser-Irradiated Targets," Appl. Phys. Lett., **24**(10), pp. 461–464.

[3] Clauer, A. H., and Holbrook, J. H., 1981, "Effects of Laser Induced Shock Waves on Metals," *Shock Waves and High Strain Phenomena in Metals—Concepts and Applications*, Plenum, New York, pp. 675–702.

[4] Peyre, P., Sollier, A., Chaieb, I., Berthe, L., Bartnicki, E., Braham, C., and Fabbro, R., 2003, "FEM Simulation of Residual Stresses Induced by Laser Peening," Eur. Phys. J.: Appl. Phys., **23**, pp. 83–88.

[5] Zhang, W., and Yao, Y. L., 2000, "Improvement of Laser Induced Residual Stress Distributions Via Shock Waves," Proc. ICALEO'00, Laser Materials Processing, Vol. 89, pp. E183–E192.

[6] Zhang, W., and Yao, Y. L., 2002, "Micro Scale Laser Shock Processing of Metallic Components," ASME J. Manuf. Sci. Eng., **124**(2), pp. 369–378.

[7] Berth, L., Fabbro, R., Peyre, P., Tollier, L., and Bartnicki, E., 1997, "Shock Waves From a Water Confined Laser Generated Plasma," J. Appl. Phys., **82**(6), pp. 2826–2832.

[8] Fabbro, R., Fournier, J., Ballard, P., Devaux, D., and Virmont, J., 1990, "Physical Study of Laser-Produced Plasma in Confined Geometry," J. Appl. Phys., **68**(2), pp. 775–784.

[9] Caruso, A., Guskov, S. Y., Doskach, I. Y., Zmitrenko, N. V., Rozanov, V. B., and Strangio, C., 2002, "Laser-Generated Weak Shock Wave Propagation Dynamics in the Solids," Proc. SPIE, **4424**, pp. 508–511.

[10] Mok, C.-H., 1968, "Effects of Solid Strength on the Propagation and Attenuation of Spherical and Plane Shock Waves," J. Appl. Phys., **39**(4), pp. 2072–2081.

[11] Clauer, A. H., Lahrman, D. F., Dulaney, J. L., and Toller, S. M., 2004, "Method Using Laser Shock Processing to Provide Improved Residual Stress Profile Characteristics," U.S. Patent No. 6,664,506.

[12] Cottet, F., and Boustie, M., 1989, "Spallation Studies in Aluminum Targets Using Shock Waves Induced by Laser Irradiation at Various Pulse Durations," J. Appl. Phys., **66**(9), pp. 4067–4073.

[13] Chen, H., Kysar, J. W., and Yao, Y. L., 2004, "Characterization of Plastic Deformation Induced by Micro Scale Laser Shock Peening," ASME J. Appl. Mech., **71**, pp. 713–723.

[14] Fan, Y., Wang, Y., Vukelic, S., and Yao, Y. L., 2005, "Wave-Solid Interactions in Laser Shock Induced Deformation Processes," J. Appl. Phys., **98**, pp. 104904[1–11].

[15] VonNumann, J., and Richtmyer, R. D., 1950, "A Method for the Numerical Calculation of Hydrodynamic Shocks," J. Appl. Phys., **21**, pp. 232–237.

[16] Assay, J. R., and Shahipoor, M., 1992, *High-Pressure Shock Compression of Solids*, Springer, New York, pp. 8–12.

[17] Zhang, W., and Yao, Y. L., 2000, "Microscale Laser Shock Processing—Modeling, Testing, and Microstructure Characterization," J. Manuf. Process., **3**(2), pp. 128–143.

[18] Johnson, G. R., Hoegfeldt, J. M., Lindholm, U. S., and Nagy, A., 1983, "Response of Various Metals to Large Torsional Strain Over a Large Range of Strain Rates," ASME J. Eng. Mater. Technol., **105**, pp. 42–53.

[19] Steinberg, D. J., Cochran, S. G., and Guinan, M. W., 1980, "A Constitutive Model for Metals Applicable at High Strain Rate," J. Appl. Phys., **51**(3), pp. 1498–1504.